Pergamon

Int. J. Heat Mass Transfer. Vol. 38, No. 2, pp. 259–266, 1995

0017-9310/95 $9.50+0.00

0017-9310(94)00161-8

Turbulent simulation of open channel flow at low Reynolds number

T. G. THOMAS and J. J. R. WILLIAMS

Turbulence Unit, Department of Civil Engineering, Queen Mary College, London E1 4NS, U.K.

(*Received* 24 *June* 1993 *and in final form* 14 *May* 1994)

Abstract—A numerical technique for simulating turbulent flows in which the free surface is allowed to undergo arbitrarily large deformations and is subject only to a maximum slope limit is applied to turbulent open channel flow at a Reynolds number of approximately 3000 based on the surface velocity and depth. The test problem has been extensively studied in the literature and allows detailed comparisons to be made. It is found that the method is in general agreement with published results and can be used for a more extensive examination of turbulent fluid mechanics at a free surface.

1. INTRODUCTION

The turbulent motion of a liquid at a free surface is much less understood than the corresponding motions at a solid boundary, but the practical applications are equally important. For example, the dispersion of pollutants in rivers and coastal waters is governed by surface phenomena. It is natural to turn to direct numerical simulation (DS) of the turbulence, and this approach is able to produce data that are more complete and often more accurate than experiments for near-wall boundary layers, but are limited to low Reynolds numbers. The large eddy simulation (LES) approach is closely related to DS but retains only the large eddies or grid scales with the smaller eddies or sub-grid scales being represented by a sub-grid model (SGM). The method thus has the disadvantage of being dependent on a model but experience has shown that the dependence is much less severe than for other methods such as k–ε or algebraic stress models. The LES approach is able to extend the Reynolds number of a simulation without increasing the computational resources required. A review of numerical simulation is given by Rogallo and Moin [1], and some recent simulations of channel flow are given by Kim *et al.* [2] and Rai and Moin [3].

An extension of the simulation techniques for wall boundary layers to include a free surface has been given by Thomas *et al.* [4]; in this paper the method is applied to an open channel at a Reynolds number of $Re^+ = 171$ (based on the wall shear velocity) and results are compared against the previous simulations of Kim *et al.* [2], and a similar simulation by Lam and Banerjee [5] which approximated the free surface using a free-slip boundary condition on a rigid upper surface. The present simulation is the first application of the free surface method to a well-documented test problem, and the objective is to verify the computer code and explore its behaviour. Once the authors are satisfied with its performance they will use the code to look in some detail at free surface turbulence.

2. COMPUTATIONAL DOMAIN

Turbulent flow is considered of an incompressible fluid of kinematic viscosity ν maintained by gravity in an infinite open channel of depth d. The Cartesian coordinates (x, y, z) are aligned with the channel such that x points in the streamwise direction, y points across the stream, and z points upwards from the bed as shown in Fig. 1. The channel slopes at a small angle α relative to the horizontal so that the flow is maintained with mean bed stress $\tau_b = \rho u_\tau^2$ where u_τ denotes the characteristic shear velocity $(\alpha g d)^{1/2}$, g denotes the acceleration due to gravity and ρ is set equal to 1. The two characteristic lengths for this flow are the depth d and the viscous length ν/u_τ which governs the structure of the flow near the bed. The ratio $u_\tau d/\nu$ is denoted Re^+ and is set equal to 171 to match the Lam and Banerjee [5] simulation and be close to the Kim *et al.* [2] simulation at $Re^+ = 180$ (certain quantities are made non-dimensional using the length ν/u_τ and are denoted by a superscript +).

The Reynolds number $Re = u_s d/\nu$ based on the mean surface velocity u_s and channel depth is given by $(u_s/u_\tau)Re^+$, where u_s/u_τ is determined from the simulation; the fine grid simulation yielded $(u_s/u_\tau) = 17.6$ and $Re = 2993$. The free surface is governed by the Froude number $Fr = u_s/\sqrt{gd}$, which can also be expressed as $\sqrt{\alpha}(u_s/u_\tau)$. The computational method imposes two constraints on the value that Fr can take: the wave slope limit requires that breaking waves cannot be tolerated and hence it is expected that Fr should be less than unity, and the size of a time-step is controlled by a Courant number based on the larger of u_s and $\sqrt{gd}$, and hence Fr must not be too small. The slope α was set to 1/1000 and hence a value of $Fr = 0.55$ was accepted. The relationship

NOMENCLATURE

c_s	subgrid constant
d	depth
D^2	discrete Laplacian
Fr	Froude number
g	acceleration due to gravity
G, H_i	rhs of finite difference equations
h	surface elevation
k	turbulence kinetic energy
K_x, K_y	wavenumber (cycles per box length)
l_x, l_y	computational box lengths
p	pressure
Re	Reynolds number, $\equiv u_s d/\nu$
Re^+	Reynolds number based on shear velocity, $\equiv u_\tau d/\nu$
S_{ij}	symmetric part of mean velocity gradient
t	time
u_s	mean surface velocity
u_τ	mean shear velocity
(u, v, w)	velocity vector
$u_{rms}, v_{rms}, w_{rms}$	rms turbulence intensities
u^+	mean velocity normalised using u_τ
$\hat{u}_i$	provisional velocity used in finite difference scheme
x, y, z	coordinates.

Greek symbols

α	channel slope
δ	finite difference operator
δ_h	characteristic amplitude of surface deformation
Δ	subgrid length scale
Δt	time step
$\Delta x, \Delta y, \Delta z$	finite difference mesh size
ε	turbulence dissipation
η	Kolmagorov length scale
κ	von Karman's constant
λ	mean streak spacing
ν	coefficient of viscosity
ν_T	coefficient of subgrid eddy viscosity
τ_b	mean bed stress, $\equiv u_\tau^2$.

between the amplitude of surface waves and the Froude number is examined in more detail in Section 8.

Following Kim and Moin [6], it was assumed that the turbulence is homogeneous in horizontal planes and use was therefore made of a computational domain with periodic boundary conditions. The lengths l_x and l_y are chosen such that the slowest decaying two-point velocity correlation is negligible over half a box length. This can be estimated initially from experimental measurements, and confirmed *a postiori* from the behaviour of the computed correlations. Kim *et al.* [2] used $l_x = 4\pi d$, $l_y = 2\pi d$ although their computed correlations suggest that the the smaller box of $l_x = 6d$, $l_y = 2d$ might be large enough. Lam and Banerjee [5] used a box of $l_x = 2\pi d$, $l_y = \pi d$. The authors have adopted $l_x = 6d$, $l_y = 2d$ which in wall units is $l_x^+ = 1026, l_y^+ = 342$ and $d^+ = 171$. Four simulations in the same size domain were run using a series of finer meshes, the coarsest of which was also run with a subgrid model. A comparison of the computational domains is presented in Table 1.

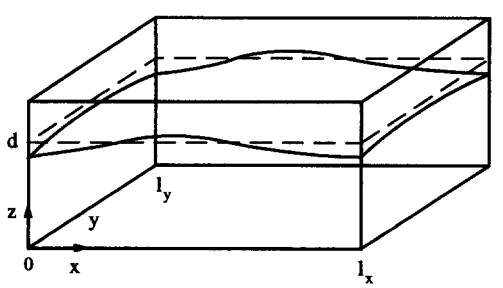

Fig. 1. Coordinate system and channel.

Ideally all scales of turbulence should be modelled down to the Kolmogorov length scale η^+, which characterises the size of the smallest, dissipating eddies. Kim *et al.* [2] estimate that the Kolmogorov scale for this flow is approximately equal to 2 and is considerably smaller than the horizontal grid resolutions: however, it appears that this degree of resolution of the turbulent motions is sufficient to achieve a realistic simulation.

3. TWO-POINT CORRELATIONS AND SPECTRA

The dominant feature of the near-wall region is the presence of low-speed streaks; these have an approximate mean spanwise spacing of $\lambda^+ = 100\nu/u_\tau$ at $z^+ = 10$ which increases with distance from the wall [7]. The two-point velocity correlations from run R3 are presented in Fig. 2(a) and (b). The slowest decays show relatively small correlations at a streamwise separation of $\frac{1}{2}l_x^+$, indicating that the computational domain has adequate length, but the correlations at a spanwise separation of $\frac{1}{2}l_y^+$ are less small and indicate that the width should be increased. The negative minimum in the $R_{uu}(r_y)$ spanwise correlation occurs at $y^+ = 40$; this implies a streak spacing of $\lambda^+ = 80$ which is the correct order of magnitude but about 20% lower than expected. This may be improved by using a slightly wider box.

The computed energy spectra for R3 are shown in Fig. 3, where K_x and K_y are measured as the number

Table 1. Computational parameters: F denotes Fourier Chebyshev modes; double entries under Δz^+ indicate (min, max) values on a stretched mesh

Run	Mesh size	l_x^+	l_y^+	Δx^+	Δy^+	Δz^+	u_s/u_τ
R0 SGM	$16\times16\times16$	1026	342	63.75	21.37	10.68	18.0
R1	$16\times16\times16$	1026	342	63.75	21.37	10.68	16.0
R2	$32\times32\times32$	1026	342	31.88	10.68	5.34	15.5
R3	$64\times64\times64$	1026	342	15.94	5.34	2.67	17.6
KMM 1987	$192\times160\times129$	2261	1130	~12	~7	(0.1, 4.4)	18.1
LB 1988	$32\times64\times65\ F$	1073	537	33	8	(0.1, 4.2)	17.9

of cycles per box length l_x and l_y, respectively. The spectra have been computed for a single time $44d/u_\tau$ and the scatter in the velocity spectra has been reduced by averaging over the depth. The energy of the high wavenumbers is many orders of magnitude less than that of the large eddies and there is no evidence of energy pile-up or aliasing errors. This confirms that there is no need of special anti-aliasing treatment. As found by Kim *et al.* [2] (hereafter denoted KMM), the different velocity components decay at the same rates with the spanwise decay more rapid than the streamwise decay. The overall decay rates are higher than those of KMM; this is expected because a finite difference discretisation of the viscous terms is generally more diffusive at higher wavenumbers than a corresponding spectral discretisation which is exact. This tendency can be reduced by increasing the resolution or using higher order spatial discretisation but it is not known to what extent the curtailment of the spectra by weak numerical damping affects the computed statistics. The evidence seems to suggest that provided the numerical damping takes effect at a wavenumber k_c such that the magnitude of fluctuations at wavenumbers $k > k_c$ is small in comparison with those at $k \ll k_c$ then the effect can be ignored. A simple analysis of the viscous term shows

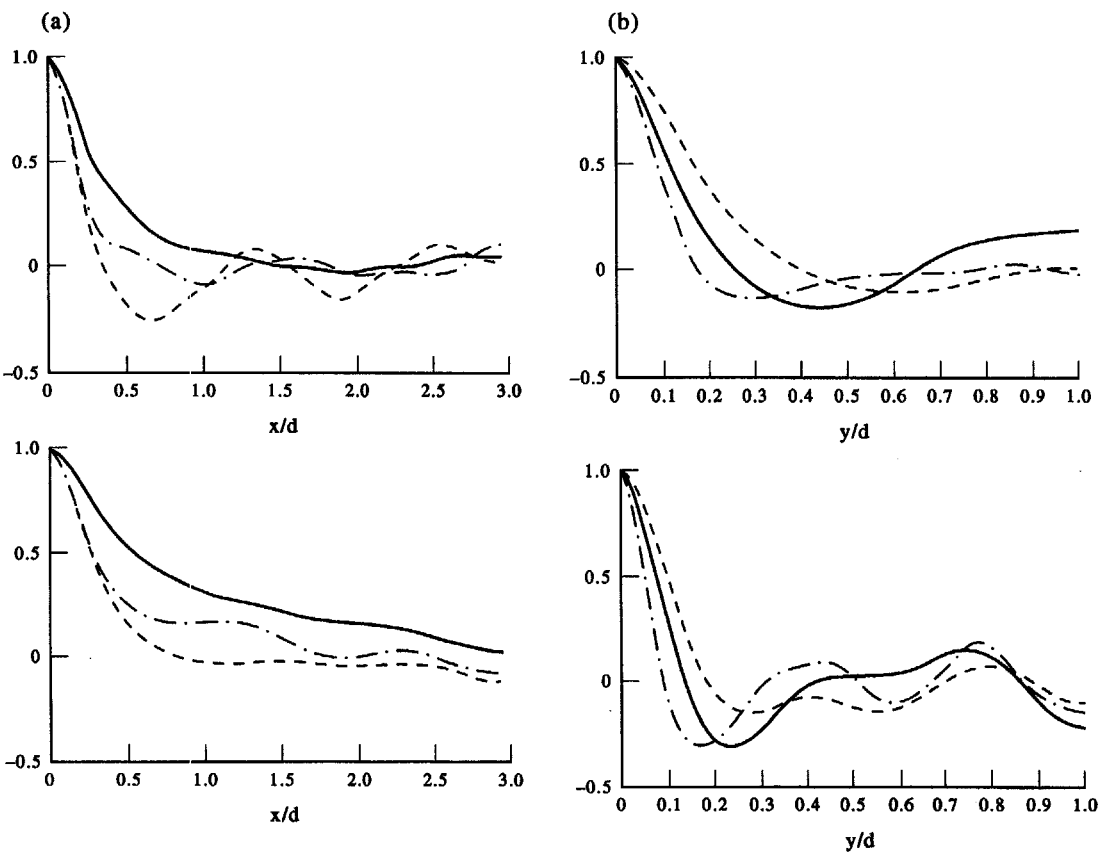

Fig. 2. (a) Two-point correlations (streamwise separations): ——, R_{uu}; – – –, R_{vv}; —·—, R_{ww}: top—$z^+ = 50$, $z/d = 0.29$; bottom—$z^+ = 12$, $z/d = 0.07$. (b) Two-point correlations (spanwise separations): ——, R_{uu}; – – –, R_{vv}; —·—, R_{ww}: top—$z^+ = 50$, $z/d = 0.29$; bottom—$z^+ = 12$, $z/d = 0.07$; minimum in R_{ww} indicates a streak spacing $\lambda^+ \approx 80$.

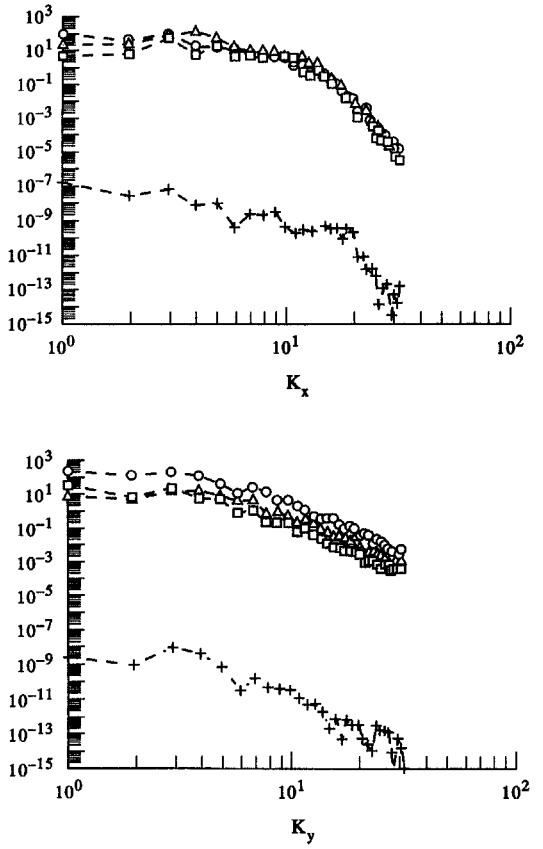

Fig. 3. Energy spectra: ○, E_{uu}; □, E_{vv}; △, E_{ww}; +, E_{hh} surface elevations. (a) streamwise; (b) spanwise (velocity correlations averaged over depth, wavenumbers K measured in cycles per box period).

that the dissipation is increased by approximately 100% above its proper value for $k\Delta x$ of about 1.5; this gives a rough estimate for k_c, and corresponds to a wavenumber K_c in Fig. 3 of approximately 15. This is relatively low and suggests that the damping is probably significant in the simulation. As engineering applications in fluid mechanics are typically for flows in non-ideal geometry for which spectral methods cannot be used it would be useful to quantify these effects more precisely.

The wave elevation spectra in Fig. 3 have not been averaged and show more scatter, also the effects of numerical truncation error are visible on both the streamwise and spanwise spectra. The spurious energy is six orders of magnitude smaller than the dominant free surface modes and is insignificant. The free surface waves are examined in more detail in Section 8.

4. NUMERICAL TECHNIQUE

The velocity field $u_i = (u, v, w)$ satisfies a discretised form of the Navier–Stokes equations and the surface elevation h satisfies $\partial h/\partial t = G$, where G is defined below. Second-order finite differences on a staggered mesh were used with an unstructured volume of fluid (VOF) type treatment at the free surface. The convection terms are approximated by central difference type operators which conserve total momentum and kinetic energy in the presence of arbitary surface deformations. The scheme requires that the local surface slope does not exceed the slope of a cell diagonal and so breaking waves cannot be simulated. This restriction has been imposed because of the computational complexity associated with different combinations of split/merged surface cells. A more comprehensive description is given in the paper by Thomas *et al.* [4]. Let us define the quantities:

$$G_i^n = \left[-\int_0^h \left(\frac{\delta u}{\delta x} + \frac{\delta v}{\delta y} \right) \mathrm{d}z \right]^n,$$

$$H_i^n = \left[-\frac{\delta u_i u_j}{\delta x_j} + \nu \mathrm{D}^2 u_i + g_i \right]^n,$$

where n denotes the discrete time level, δ the finite difference operator, D^2 the discrete Laplacian. The time advancement scheme used originally was only first-order accurate and although it conserved the potential energy of surface waves it proved to be unsuitable for simulating turbulence. It is necessary that the time truncation error associated with the convection terms be very small compared with the viscous dissipation term, and this could be satisfied only for unacceptably small time steps. A combination of an Adams–Bashforth scheme for the momentum terms and a Crank–Nicholson scheme for the surface elevation was finally used; this is not strictly conservative of wave energy but is able to simulate both turbulence and free surface waves accurately provided that the Courant numbers $u\Delta t/\Delta x$ and $\sqrt{gd}\Delta t/\Delta x$ are small. The solution is advanced over a timestep using the equations:

$$\frac{\hat{u}_i - u_i^n}{\Delta t} = \frac{3}{2} H_i^n - \tfrac{1}{2} H_i^{n-1} + \frac{1}{2} \frac{\delta p^{n-1}}{\delta x_i}, \tag{1}$$

$$\frac{u_i^{n+1} - \hat{u}_i}{\Delta t} = -\frac{3}{2} \frac{\delta p^n}{\delta x_i}, \tag{2}$$

$$\mathrm{D}^2 p^n = \frac{2}{3\Delta t} \frac{\delta \hat{u}_j}{\delta x_j}, \tag{3}$$

$$\frac{h^{n+1} - h^n}{\Delta t} = \tfrac{1}{2} G^{n+1} + \tfrac{1}{2} G^n, \tag{4}$$

where $\hat{u}_i$ denotes an intermediate variable. The continuity equation $\delta u_j^{n+1}/\delta x_j = 0$ is enforced at time level $n+1$ and is equivalent to the Poisson equation (3) for the pressure p. First, $\hat{u}_i$ is computed using equation (1) and then p^n is determined such that u_i^{n+1} satisfies continuity by solving equation (3). The boundary conditions are assumed built in to the difference operators and need not be explicitly treated. The finite difference form of D^2 produces a 15-point star at the free surface which reduces to the usual 7-point star in the interior and the resulting system of equations were solved using an SOR method with red–black labelling in

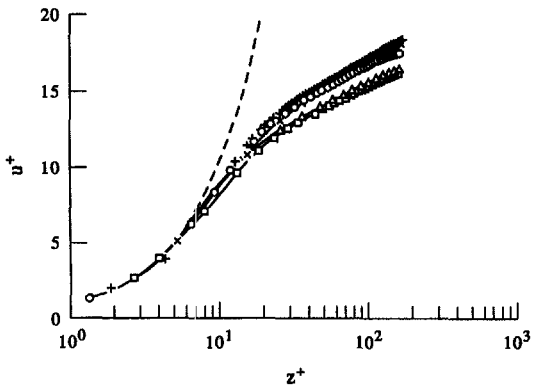

Fig. 4. Mean velocity profiles: ○, R3 64 × 64 × 64 mesh; □, R2 32 × 32 × 32 mesh; △, R1 16 × 16 × 16 mesh; ×, R0 16 × 16 × 16 mesh and subgrid model; +, Nishino and Kasagi [8], experimental data; ∇, Lam and Banerjee [5], computed data $30 \leqslant z^+ \leqslant 130$; ---, $u^+ = z^+$.

horizontal planes to enable vectorisation and Gauss–Siedel treatment vertically. In practice the SOR method is much faster than might be expected: the iteration starts with the last known pressure as an initial approximation, and in a turbulent flow the large-scale features of p change relatively slowly compared with the small-scale features; and this is well matched to the known convergence rates of SOR at different scales. It appears that under the circumstances of the simulation relatively few iterations are needed at each time step. Once p is determined, the new velocity is updated using equation (2). The new surface elevation h^{n+1} is found from equation (4) which is weakly non-linear in that G^{n+1} depends on h^{n+1} and is solved by iteration and converges rapidly. The overall scheme has been tested successfully on simple laminar flows and free surface solitons. The subgrid model used in R0 was a standard Smagorinsky model: the viscosity ν is enhanced by an eddy viscosity ν_T defined as:

$$\nu_T = (C_s\Delta)^2(2S_{ij}S_{ij})^{1/2},$$

where S_{ij} denotes the symetric part of the mean velocity gradient, Δ the cube root of the cell volume, and C_s a model constant taken as equal to 0.15.

The simulation was started from an initial semi-parabolic profile with superimposed random numbers to create an artificial turbulence field and was integrated over time for $36d/u_\tau$ until a statistically steady or fully developed turbulent flow was indicated by the total stress (see Fig. 5). A timestep $\Delta t = 0.0005d/u_\tau$ was used for run R3; the coarser mesh runs were scaled to use the same Courant numbers. Statistics were averaged over a further $8d/u_\tau$.

5. MEAN VELOCITY

The mean velocity profile $u^+ = u_m/u_\tau$ normalised by the wall shear velocity is shown in Fig. 4. Within the laminar sublayer $z^+ < 6$ the profiles converge onto the the linear law $u^+ = z^+$, and beyond $z^+ > 30$ show logarithmic behaviour. The computed profile from run R3 closely follows the log-law $u^+ = \kappa^{-1}\ln(z^+) + 5.6$, where the von Karman constant is determined as $\kappa = 0.41$. There is evidence of a wake region near the free surface associated with the boundary condition $du^+/dz = 0$ at $z^+ = Re^+$. The mean velocity computed by Lam and Banerjee [5] (hereafter denoted LB), is plotted in the interval $30 < z^+ < 130$ and coincides almost exactly with the R3 profile except in the near surface region $z^+ > 130$ (not shown) where it follows the log-law. The experimental data of Nishino and Kasagi [8] agree quite closely with the above log-law but are consistently about 2.5% higher in the logarithmic region. The differences in the wake region are expected because the different value of Re implies that the symmetry boundary condition is imposed at a higher z^+ value. The profiles from the lower resolution runs R1 and R2 exhibit the correct logarithmic behaviour but are typically 7% too low and suggest that these meshes are too coarse. It is surprising that the subgrid model used in run R0 is able to correct the profile of R1 to the extent that it follows the computed profile of R3 in the logarithmic region up to the start of the wake region. It is of some engineering interest to quantify the coarsest (or least expensive) mesh that can be used for reliable computation of certain features of turbulent flows but the quality of the other R0 statistics are considered too poor to be useful.

6. REYNOLDS STRESS

The Reynolds shear stress $-\langle u'w'\rangle/u_\tau^2$ normalised by the wall shear velocity u_τ^2 is shown in Fig. 5. Also plotted is the total stress $-\langle u'w'\rangle/u_\tau^2 + (1/Re^+)du^+/dz^+$, used to indicate the state of development of the flow, and the absence of any significant deviations from a straight line confirms that the flow is fully developed.

The computed Reynolds stress from run R3 is in excellent agreement with the KMM simulation ($Re^+ = 180$), both show a peak of 0.72 at $z^+ = 30$.

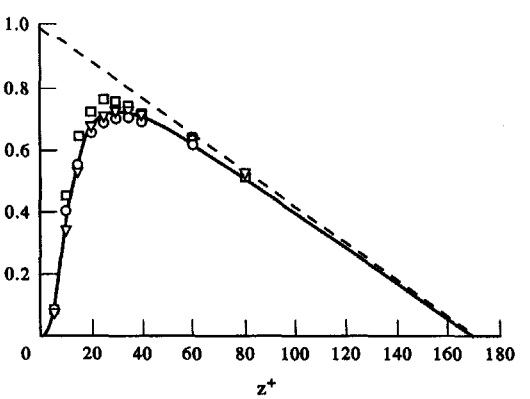

Fig. 5. Reynolds stress: ——, $-\langle u'w'\rangle/u_\tau^2$ R3; ---, $-\langle u'w'\rangle/u_\tau^2 + (1/Re^+)du^+/dz^+$ R3; □ Lam and Banerjee [5] $Re^+ = 171$; ∇, Kim *et al.* [2], $Re^+ = 180$; ○, Nishino and Kasagi [8], experimental $Re^+ = 205$.

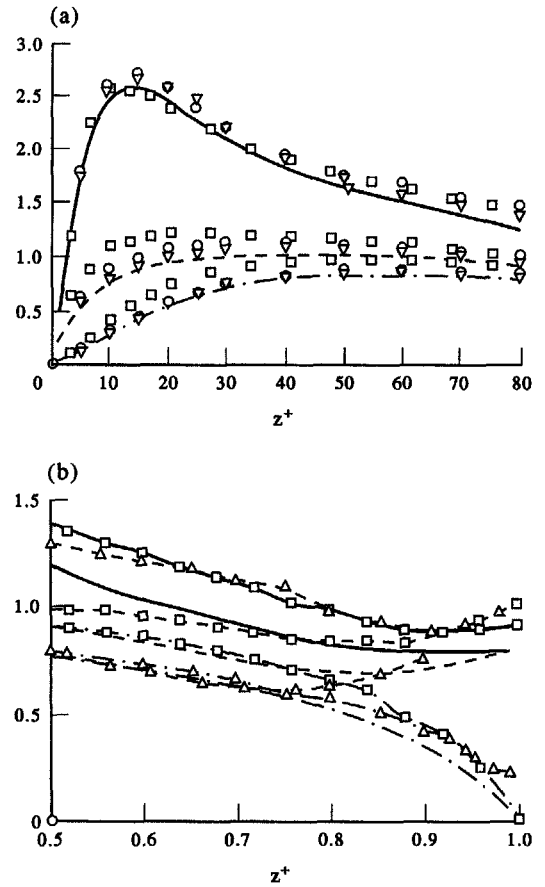

Fig. 6. (a) Turbulent intensities (lower part of channel): ——, u_{rms}/u_τ; – – –, v_{rms}/u_τ; — · —, w_{rms}/u_τ; □, Lam and Banerjee [5], *computed* $Re^+ = 171$; ▽, Kim *et al.* [2], *computed* $Re^+ = 205$; ○, Nishino and Kasagi [8] *experimental* $Re^+ = 180$. (b) Turbulent intensities (upper part of channel): ——, u_{rms}/u_τ; – – –, v_{rms}/u_τ; — · —, w_{rms}/u_τ; □, Lam and Banerjee [5], *computed* $Re^+ = 171$; △, Komori *et al.* [2], *experimental* $Re^+ = 176$.

The experimentally observed Reynolds stresses of Nishino and Kasagi [8] are in good agreement with the computed values, but show a slightly lower peak of 0.70 at the same $z^+ = 30$. The LB computed stresses ($Re^+ = 171$) show good overall agreement, but the peak is higher at 0.76 and closer to the wall at $z^+ = 25$. All the profiles agree in the near wall region $z^+ < 25$. KMM noted that the experimental measurements of Eckelmann [9] were too high relative to the computed values in this region and asymptotic analysis of the near wall flow suggested that the measurements might be unreliable this close to the wall. The newer measurements made by Nishino and Kasagi [8] seem to correct this.

7. TURBULENCE INTENSITIES

The turbulence intensities normalized by the bed shear velocity are shown in Fig. 6(a) and (b) for the near-bed region and near-surface regions, respectively. The computed intensities from the LB and KMM simulations are included and comparisons are made against the experimental measurements of Nishino and Kasagi [8] and Komori *et al.* [10].

Near the bed, the experimental and KMM u_{rms} profiles are in good agreement, and the LB profile has a slightly lower peak value located nearer to the bed. The profile from run R3 also has a slightly lower peak value but in the same position as KMM: however, the tail away from the bed is about 10% lower than the consensus. The agreement between v_{rms} profiles of KMM and run R3 is good, but is about 10% lower than the experimental measurements. The LB profile is considerably higher than the consensus for $z^+ < 40$ but shows much better agreement further away from the wall. There is excellent agreement amongst the w_{rms} profiles of run R3, KMM, and the experimental measurements, but the LB profile is again considerably above this.

Near the surface the overall agreement is less good; the overall shape of the profiles are similar but the magnitudes differ by up to 15%. Part of the discrepency is due to differences amonst the intensities in the middle depth away from the surface influence: the R3 u_{rms} is clearly too low, the LB v_{rms} and w_{rms} are too high. Although some of the profiles are in very good agreement, the overall agreement is relatively poor and more work needs to be done to establish a generally accepted set of profiles as is the case with the wall region.

The effect of the free surface is to increase the intensity of the streamwise and spanwise fluctuations in a thin layer close to the surface; the simplest explanation is that the presence of the impermeable boundary constrains the fluid motions to be parallel to it, and these motions contribute to the corresponding rms intensities. The thickness of the layer is an integral measure of the eddy size.

The increases at the surface are much stronger in the experimental measurements than in the computed results and could be exaggerated by experimental error. LB have noted out that the experimental w_{rms} measurements tend to a constant, approximately equal to $0.2u_\tau$, at the surface which suggest that ordinary water waves are present. If it is assumed that the wavelength is small compared with the depth, and hence that the particle orbits are circular, then there must be a similar enhancement of the measured horizontal intensities.

The measurements of v_{rms} and w_{rms} of Komori *et al.* [10] are also not consistent with those of Nishino and Kasagi [8] where they overlap in the middle depth. It is possible that the differences may be due the different physical boundary conditions in place, i.e. channel centreline and free-slip surface.

8. SURFACE ELEVATION

A view of the free surface elevation $h(x, y)$ normalized by depth d is shown in Fig. 7 for time $44d/u_\tau$.

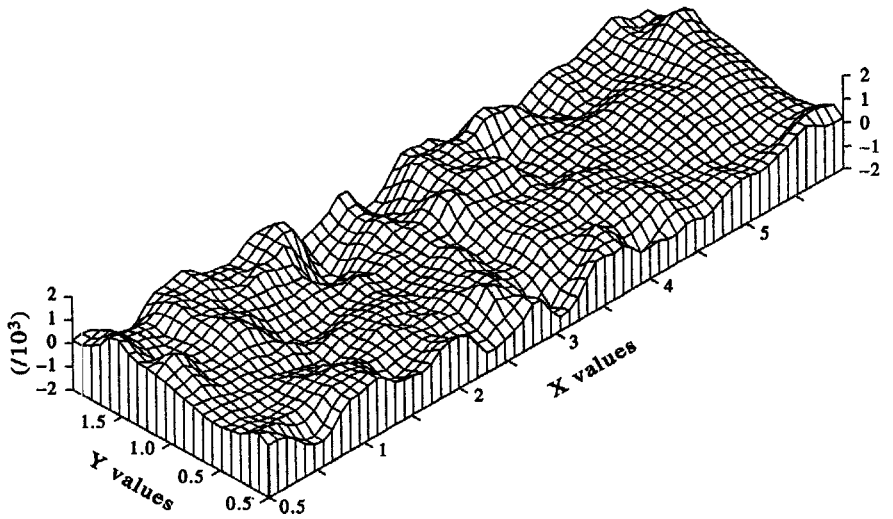

Fig. 7. Surface elevation $h(x, y)$ normalised by depth at time $44d/u_\tau$.

The largest waves are those with their crests aligned normal to the streamwise direction, but spanwise waves are also present. The dominant modes (K_x, K_y) can be seen from the energy spectra (see Fig. 3) to be the $(1, 0)$ and $(3, 0)$ modes, and overall the spanwise modes are much less energetic than the streamwise modes. The dominance of the streamwise modes implies special forms for the surface elevation auto-correlations: the spanwise correlation $R_{hh}(y)$ does not decay significantly and remains near to unity across the flow; the streamwise correlation $R_{hh}(x)$ oscillates and is significantly negative at the maximum separation. In the present paper the waves are treated simply as surface deformations induced by turbulent eddies in the underlying flow; the authors have made no attempt to separate time dependent components. The characteristic size of the surface deformation δ_h is determined by equating the potential energy $g\delta_h$ with the kinetic energy $\frac{1}{2}u_\tau^2$, where it is supposed that the vertical velocity of a typical eddy is approximately equal to u_τ, so that after some rearrangement:

$$\frac{\delta_h}{d} = \frac{1}{2}\alpha = \frac{1}{2}Fr^2\left(\frac{u_\tau}{u_s}\right)^2.$$

The wave height δ_h is thus directly related to the bed slope α and is very small ($\delta_h = 0.0005d$ in the present simulation). The second part of the equation shows that δ_h varies with the square of the Froude number when the Reynolds number is kept constant. The computed root-mean-square surface elevation h_{rms} taken at time $44d/u_\tau^*$ is equal to $1.14\delta_h$ and is in excellent agreement with the above estimate.

The results suggest that streamwise waves with long spanwise correlation lengths might be a stable feature of real turbulent flows.

9. TURBULENT KINETIC ENERGY EQUATION

Figure 8 shows the computed profile of terms in the turbulent kinetic energy equation:

$$-\langle u_i'u_j'\rangle\frac{\partial\langle u_i\rangle}{\partial x_j} - \nu\left\langle\frac{\partial u_i'}{\partial x_j}\frac{\partial u_i'}{\partial x_j}\right\rangle + \left\langle p'\frac{\partial u_i'}{\partial x_i}\right\rangle - \frac{\partial}{\partial x_j}\left[\tfrac{1}{2}\langle u_i'u_i'u_j'\rangle + \langle p'\delta_{ij}u_i'\rangle\right] + \frac{\nu}{2}\nabla^2\langle u_i'u_i'\rangle = 0,$$

for the velocity component i (repeated index i not summed). The terms are normalized by u_τ^4/ν and only the streamwise ($i = 1$) component is plotted; the other component terms are small in comparison. The production term has its maximum value 0.23 at $z^+ = 12$ which is about 23% lower than the maximum of 0.30 located at $z^+ = 10$ computed by Lam and Banerjee [5]. Very near to the wall $z^+ < 5$ the dissipation is balanced by viscous diffusion of kinetic energy from the maximum production region; further out the diffusion processes are less significant and the main balance is between the losses to dissipation and pressure strain mediated exchange and the production. The pressure strain term is negative; this is the pri-

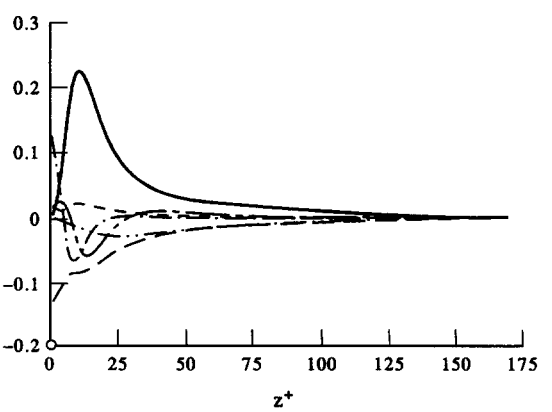

Fig. 8. Terms of the turbulent kinetic energy equation for $\frac{1}{2}\langle u^2\rangle$ normalised by u_τ^4/ν: ——, production; — — —, turbulent diffusion; — · —, viscous diffusion; — · · —, pressure strain; — — — —, dissipation; – – –, residual error.

mary source of spanwise and vertical components of turbulent kinetic energy because the production term for these must vanish. LB found that very near to the free surface the pressure strain term became slightly positive; this is consistent with the idea that at the free surface any vertical motion would tend to be redirected into the horizontal plane and hence appear as a source for streamwise kinetic energy. The authors have not examined this point. The overall agreement with LB is good to the extent that the computed profiles look very similar but the magnitudes are consistently about 23% lower. This may be due to the use of a relatively coarse mesh and a simulation on a finer mesh is planned to be carried out.

10. SUMMARY AND CONCLUSIONS

A first simulation of a turbulent open channel flow at a Reynolds number of $Re^+ = 171$ and Froude number of $Fr = 0.55$ was performed using a relatively coarse mesh of $64 \times 64 \times 64$ and a slightly restricted computational box but allowing unconstrained movement of the free surface. The numerical scheme used conventional finite differences on a staggered mesh for interior points but with the unstructured mesh technique described by Thomas *et al.* [4] applied to fluid cells near to the free surface. The method was designed to conserve mass, momentum, and kinetic energy to the same extent as a conventional turbulence code, and to be capable of simulating large amplitude laminar and inviscid wave motions. The results have been compared with previous simulations at a similar Reynolds number of a symmetric channel flow [2] and a half channel with an impermeable and free-slip rigid lid [5], and with the experimental measurements of Nishino and Kasagi [8] and Komori *et al.* [10].

A series of meshes have been used starting from a $16 \times 16 \times 16$ mesh but it is felt that only the $64 \times 64 \times 64$ (R3) mesh provided acceptable results, the others being too coarse, and the authors intend to perform a finer simulation with more points to confirm the preliminary results. The results also suggest that the computational box should be made slightly larger. The energy spectra show no evidence of energy pile-up and confirm that the numerical scheme is stable, but show more rapid decay than expected at high wavenumbers: it is believed that this extra dissipation is due to using finite difference rather than spectral approximations. The agreement with published numerical and experimental data is in general very good. The worst agreement is for the root-mean-square velocity fluctuations on approaching the free surface, but the Komori *et al.* [10] experimental measurements of this appear to be contaminated by excessive surface waves and are not consistent with the Nishino and Kasagi [8] measurements in the middle depth of the channel. The simulation suggests that streamwise surface waves with significant spanwise correlation and (rms) amplitude of half the channel slope times the depth may be a stable feature of turbulent open channel flow.

Acknowledgements—This work was carried out under grant GR/F88995 from the U.K. Science and Engineering Research Council and National Power plc, whose support the authors gratefully acknowledge.

REFERENCES

1. R. S. Rogallo and P. Moin, Numerical simulation of turbulent flows, *Ann. Rev. Fluid Mech.* **16,** 99 (1984).
2. J. Kim, P. Moin and R. Moser, Turbulence statistics in fully developed flow at low Reynolds number, *J. Fluid Mech.* **177,** 133–166 (1985).
3. M. M. Rai and P. Moin, Direct simulations of turbulent flow using finite difference schemes, *J. Comp. Phys.* **96,** 15–53 (1991).
4. T. G. Thomas, J. J. R. Williams and D. C. Leslie, Development of a conservative 3D free surface code, *J. Int. Ass. Hydraul. Res.* **30,** 107–115 (1992).
5. K. Lam and S. Banerjee, Investigation of turbulent flow bounded by a wall and free surface. In *Fundamentals of Gas–Liquid Flows*, Proc. ASME Ann. Mtg, Chicago (1988).
6. J. Kim and P. Moin, The structure of the vorticity field in turbulent channel flow. Part 2. Study of ensemble-averaged fields, *J. Fluid Mech.* **162,** 339 (1985).
7. C. R. Smith and S. P. Metzler, The characteristics of low-speed streaks in the near-wall region of a turbulent boundary layer, *J. Fluid Mech.* **129,** 27 (1983).
8. K. Nishino and N. Kasagi, Turbulence statistics measurement in a two-dimensional channel flow using a three-dimensional particle tracking velocimeter. *Seventh Symposium on Turbulent Shear Flows*, Stanford University **2,** 1063–1075 (August 1989).
9. H. Eckelmann, The structure of the viscous sublayer and the adjacent wall region in a turbulent channel flow, *J. Fluid Mech.* **65.** 439 (1974).
10. S. Komori, H. Ueda, F. Ogino and T. Mizushina, Turbulence structure and transport mechanism at the free surface in an open channel flow, *Int. J. Heat Mass Transfer* **26,** 513–521 (1982).